Research Square

Preprints are preliminary reports that have not undergone peer review.
They should not be considered conclusive, used to inform clinical practice,
or referenced by the media as validated information.

Lgals3 governs muscle satellite cell quiescence and regeneration via Drp1-dependent mitochondrial dynamics

Zhiyin Liao

241036@cqmpc.edu.cn

Chongqing Medical and Pharmaceutical Colleage

Zhiyin Liao

The First Affiliated Hospital of Chongqing Medical University

Minghan Xiao

ChongQing Medical University

Article

Keywords: Lgals3, muscle satellite cells, mitochondrial fission, Drp1, autophagy, skeletal muscle regeneration

Posted Date: October 21st, 2026

DOI: https://doi.org/10.21203/rs.3.rs-11180171/v1

License: This work is licensed under a Creative Commons Attribution 4.0 International License.
Read Full License

Additional Declarations: (Not answered)

Abstract

The regulatory mechanism of muscle satellite cells (MuSCs) and their relationship with Lgals3 remain unclear. Here, we generated MuSC-specific Lgals3 knockout (Lgals3scko) mice and evaluated the effects on skeletal muscle regeneration, MuSC activation, proliferation, differentiation, self-renewal, mitochondrial morphology, ATP production, autophagy, and Lgals3–Drp1 interaction. Lgals3 was absent in quiescent MuSCs and induced upon activation. Lgals3scko mice exhibited impaired muscle regeneration with reduced CSA and CNF numbers ($P < 0.05$). Lgals3 deletion reduced MuSC activation, proliferation, and differentiation ($P < 0.05$), enhanced self-renewal ($P < 0.05$), increased mitochondrial fission ($P < 0.05$), decreased ATP levels ($P < 0.05$), and promoted autophagy ($P < 0.05$). Lgals3 interacted with Drp1, and double depletion restored mitochondrial morphology. Through Drp1-mediated mitochondrial fission and autophagy, Lgals3 may act as a molecular switch between self-renewal and differentiation, thereby regulating MuSC fate and muscle regeneration.

Introduction

Muscle atrophy is a pathological condition caused by disuse, malnutrition, and a variety of diseases (such as sarcopenia, diabetes, cancer, and HIV infection[1–4]), which affects millions of patients worldwide. Currently, no effective treatment exists for disease-induced muscle atrophy. Skeletal muscle regeneration is a critical process for maintaining muscle function and tissue integrity, in which muscle satellite cells (MuSCs) play a central role as the adult stem cells of skeletal muscle[5]. MuSCs reside between the sarcolemma and the basement membrane of muscle fibers. In steady-state muscle, MuSCs are typically quiescent, a reversible resting state in the G0 phase of the cell cycle. Upon muscle damage, MuSCs become activated and initiate a regeneration program, which involves activation, proliferation, differentiation into myoblasts, and their ultimate fusion to repair or replace damaged muscle fibers[6]. Concurrently, a portion of the progenitor cells exit the cell cycle to self-renew; these cells are subsequently incorporated back into the satellite cell population beneath the basement membrane to maintain a reservoir for future rounds of damage[7]. Functional impairment of MuSCs has been established as a contributing factor in various muscle diseases[8]. In genetic muscle diseases such as Duchenne muscular dystrophy, MuSCs exhibit significant depletion[9] and impaired self-renewal[5]. In contrast, age-related muscle diseases, such as sarcopenia or a decline in regeneration capacity, are associated with MuSC senescence[10, 11] and dysregulation of cell cycle dynamics[12].

Although the core role of MuSCs in skeletal muscle regeneration has been widely studied, their regulatory network remains incompletely elucidated. The mechanisms by which MuSCs fine-tune the transition between quiescent and activated states, as well as the balance between proliferation and differentiation, remain poorly understood. Furthermore, MuSCs exhibit limited expansion potential in vitro, and traditional culture conditions fail to maintain their undifferentiated state, leading to rapid differentiation into myoblast progenitor cells and a consequent loss of regenerative capacity[13]. This

limitation presents a major obstacle for their application in cell therapy, particularly for the treatment of diseases such as muscle atrophy[14, 15].

The galectin family comprises soluble β-galactoside-binding lectins that regulate diverse physiological and pathological processes, including inflammation, cell–cell and cell–matrix interactions, and membrane fusion during myogenesis[16]. Among them, galectin-1 is the most extensively studied in muscle differentiation[17], where it governs muscle repair and development[18–20]. whereas galectin-3 (Lgals3) has recently been shown to enhance muscle regeneration in C2C12 cells and to impair regeneration upon knockout in mouse skeletal muscle[21, 22]. As the only chimeric galectin, Lgals3 participates in cell cycle regulation, apoptosis, autophagy, inflammation, and energy metabolism[23–25], yet its role in muscle satellite cells remains unclear.

This study aimed to investigate the function of Lgals3 in MuSCs and its regulatory mechanisms during skeletal muscle regeneration. By analyzing Lgals3 expression patterns and its regulatory impact on MuSC fate, we demonstrate a key role for Lgals3 in MuSC activation and skeletal muscle regeneration. Moreover, our findings reveal a molecular mechanism by which Lgals3 maintains the activated state of MuSCs by regulating mitochondrial fission and autophagy. This discovery enhances the theoretical understanding of MuSC fate determination and identifies new potential targets for the development of MuSC-based cell therapies.

Materials/Subjects and Methods

Animals

All mouse strains were procured from Shanghai Model Organisms Center, Inc.(*Pax7*^{CreERT2}, Cat. NO. NM-KI-200099;*Lgals3*^{fl}, Cat. NO. NM-CKO-220404), Lgals3^{scko} were generated by crossing *Pax7*^{CreERT2} and *Lgals3*^{fl} mice, with genotyping determined by tail DNA PCR. Housing, feeding, and all experimental procedures were approved by the Animal Care and Use Committee of Chongqing Medical University (Approval number: K2023-085). To induce Cre activity, tamoxifen (10 mg/ml in corn oil) was administered i.p. for 5 consecutive days (100 mg/kg/d) at 8 weeks of age and kept on tamoxifen-containing standard chow for the duration of the experiment. To induce skeletal muscle injury, CTX (10 μM, 100 μL, MCE) was injected into TA muscles at the age of 12 weeks[26].

Isolation and cultivation of single muscle fibers

Single muscle fibres were isolated as previously described[27]. Briefly, isolated mouse hindlimb EDL muscles were digested at 37°C for approximately 90 minutes in a cell culture incubator in serum-free Ham's F-10 media supplemented with 400 U/mL collagenase II (Biosharp, BS164) and 1% Penicillin-Streptomycin (Pen/Strep). Single muscle fibres were released by gentle pipetting using a sterile glass Pasteur pipette pre-coated with horse serum and were subsequently transferred under microscopic

observation. The fibres were then transferred to horse serum-pre-coated 6-well plates, suspended in F-10 media supplemented with 20% fetal bovine serum (FBS) and 1% Pen/Strep, and cultured at 37°C in a 5% CO_2 atmosphere. For the analysis of quiescent satellite cells, fibres were immediately fixed with 4% paraformaldehyde (PFA) and then processed for staining. To investigate satellite cell activation, fibres were harvested at specified time points.

Isolation and cultivation of MuSCs

Hindlimb muscles were dissected from mice, minced into a suspension, and digested in Ham's F-10 medium containing 800 U/mL collagenase II (Biosharp, BS164) and 1% Pen/Strep at 37°C with agitation at 60 rpm for 1 h. Subsequently, the digested tissue was further digested in Ham's F-10 medium containing 100 U/mL collagenase II, 2 U/mL dispase (Biosharp, BL1360A), and 1% Pen/Strep for 30 min under the same conditions. The resulting suspension was mechanically dissociated by repeated passage through a 20G needle. The cells were then stained with antibodies against PE-Cy™7-CD45 (#552848, BD Pharmingen), APC-CD31 (#102510, Biolgend), FITC-CD34 (#11-0341-85, eBioscience), and PE-α7-integrin (#MA5-23608, Thermo Fisher Scientific). MuSCs ($CD31^{-}CD45^{-}\alpha7\text{-integrin}^{+}CD34^{+}$) were isolated using fluorescence-activated cell sorting (FACS). Sorted MuSCs were immediately centrifuged, resuspended in F10 media supplemented with 20% FBS and 1% Pen/Strep, and plated onto culture dishes pre-coated with Matrigel (Yeasen), and cultured at 37°C in a 5% CO_2 atmosphere.

Isolation and cultivation of primary myoblasts

Hindlimb muscles were digested in PBS with collagenase II (Biosharp, BS164, 50 U/mL) for 45 min, then in collagenase II (Biosharp, BS164, 0.1 U/mL) plus dispase (Biosharp, BL1360A, 0.8 U/mL) for 30 min. The suspension was sequentially filtered through 70 μm and 40 μm strainers, centrifuged, and plated on uncoated dishes. After 1 h, non-adherent cells were transferred to 1% gelatin-coated dishes. Following overnight incubation, adherent muscle mononuclear cells were incubated on ice for 30 min to detach cells, which were then collected and plated on Matrigel-coated Petri dishes. Complete growth medium (DMEM with 20% FBS, 1% Pen/Strep) was changed every two days. Cells were passaged with trypsin before confluence to prevent differentiation, and cells cultured for no more than 1 month (6–15 passages) were used. For myoblast differentiation, at 80% confluence, growth medium was replaced with differentiation medium (DMEM with 2% horse serum, 1% Pen/Strep).

H&E Staining and Morphological Analysis

To evaluate skeletal muscle morphology and regeneration, tibialis anterior (TA) muscles were fixed in 4% formalin for 24 h, paraffin-embedded, and cut into 5 μm thick transverse sections. Following deparaffinization in xylene, sections were rehydrated through a graded ethanol series and subsequently stained with hematoxylin and eosin (H&E). For quantitative analysis, the cross-sectional area (CSA) and

the number of centronucleated fibers (CNF) were quantified on H&E-stained TA muscle sections using ImageJ software.

Immunofluorescence

For tibialis anterior (TA) muscle sections: Dewaxing was performed in xylene, followed by dehydration through a graded ethanol series. Antigen retrieval was conducted via microwave treatment in Tris-EDTA buffer (pH 8.0). After washing with PBS, sections were blocked with 3% bovine serum albumin (BSA) for 1 hour at room temperature. Sections were then incubated overnight at 4°C with primary antibodies against Pax7 (mouse, 1:20, #Pax7, DSHB) and Laminin (rabbit, 1:1000, #L9393, Sigma).

For isolated single muscle fibers and cells: Samples were fixed in 4% paraformaldehyde (PFA) for 15 minutes at room temperature, washed, and subsequently incubated with 0.1 M glycine for 10 minutes to quench the fixation. Next, samples were permeabilized with 0.5% Triton X-100 for 10 minutes, washed with PBS, and blocked in a solution containing 3% BSA, 0.2% Triton X-100, and 5% horse serum for 1 hour at room temperature. These samples were then incubated overnight at 4°C with primary antibodies, including those against Pax7 (mouse, 1:20, #Pax7, DSHB), Lgals3 (rabbit, 1:100, #14979-1-AP, Proteintech), Myod1 (rabbit, 1:300, #ab133727, Abcam), Myogenin (mouse, 1:100, #F5D, DSHB), and myosin heavy chain (MyHC; mouse, 1:50, #F1.652, DSHB).

For all samples, after primary antibody incubation and a PBS wash, samples were incubated with corresponding secondary antibodies for 1 hour at room temperature. Subsequently, nuclei were counterstained with DAPI.

Cell proliferation assay

Cell proliferation was assessed using the EdU Cell Proliferation Image Kit (Abbkine, KTA2031) according to the manufacturer's protocol. Briefly, cells were plated onto Matrigel-coated glass coverslips in a 24-well plate and incubated at 37°C in a 5% CO2 atmosphere for 48 hours. To label proliferating cells, EdU was added at final 2 hours.

Analysis of Mitochondrial Morphology

Mitochondria were stained with Mito-Tracker Red CMXRos (Beyotime, C1035). After 24 hours of culture on Matrigel-coated coverslips in a 24-well plate (37°C, 5% CO2), the cells were incubated with the Mito-Tracker working solution for 30 minutes. Subsequently, cells were washed with PBS, fixed with 4% PFA for 15 minutes, nuclei were counterstained with DAPI. Mitochondrial morphology was analyzed using ImageJ software as previously described[28].

ATP level detection

ATP levels were assessed using an ATP Assay Kit (Beyotime, S0026) according to the manufacturer's protocol. Briefly, cells were seeded in 6-well plates, grown to appropriate density, lysed in 200 μL lysate per well with repeated pipetting, and centrifuged at 12,000 rpm for 10 min at 4°C. The supernatant was collected for protein quantification. ATP standards (0.01–10 μM) were prepared, and working solution was made by diluting ATP detection reagent with diluent (1:9). A 96-well plate was loaded with 100 μL working solution per well (samples in duplicate) and incubated at room temperature for 3–5 min to deplete background ATP. Then, 20 μL of sample or standard was added, mixed, and RLU was measured after ≥ 2 s. ATP concentration was calculated from the standard curve and normalized to protein concentration (nmol/mg protein).

Western blotting

Cells were homogenized in radioimmunoprecipitation assay (RIPA) buffer (Beyotime) supplemented with protease and phosphatase inhibitor cocktails (Beyotime). Total protein concentration was quantified using a bicinchoninic acid (BCA) assay kit (Beyotime). Equal amounts of protein were then separated by sodium dodecyl sulfate–polyacrylamide gel electrophoresis (SDS-PAGE) and electrophoretically transferred to a polyvinylidene fluoride (PVDF) membrane. Immunoblotting was performed according to standard protocols. For immunoblotting, the following primary antibodies were used: anti-Lgals3 (rabbit, 1:1000, #14979-1-AP, Proteintech), anti-Drp1 (rabbit, 1:1000, #12957-1-AP, Proteintech), anti-P62 (rabbit, 1:1000, #WL02385, Wanleibio), anti-cleaved-caspase-3 (rabbit, 1:1000, #WL01992, Wanleibio), anti-LC3 (rabbit, 1:1000, #WL01506, Wanleibio), and anti-GAPDH (rabbit, 1:1000, #60004-1-Ig, Proteintech).

Co-IP

After protein extraction and concentration measurement, 1 mg of total protein was transferred to an EP tube and incubated overnight at 4°C with 1 μg of anti-Lgals3 (rabbit, 1:1000, #14979-1-AP, Proteintech). Then, 100 μL of protein G beads (Proteintech) was added and incubated at 4°C for 2 h. The beads were washed five times with pre-cooled PBS containing protease inhibitor (100:1). After the final wash, 80 μL of wash solution was retained, and 20 μL of 5× SDS loading buffer was added. The beads were suspended, boiled, and centrifuged, and the supernatant was used for subsequent immunoblotting.

siRNA transfection

siRNA targeting Drp1 was designed and synthesized by GeneCopoeia. Cells were seeded in 24-well plates and grown to an appropriate density, after which the medium was replaced with 200 μL of fresh medium per well and the plates were returned to the incubator. For each well, transfection mixtures were prepared in two separate tubes: 50 μL of Opti-MEM I (Gibco) with 1 μL of siRNA or empty virus (GeneCopoeia), and 50 μL of Opti-MEM I with 1 μL of EndoFectin-MAX (GeneCopoeia). Both mixtures were gently mixed and incubated at room temperature for 5 min. The two solutions were then combined (100 μL total) and incubated at room temperature for 20 min. The mixture was added dropwise to each well with gentle agitation, and the plates were returned to the incubator. Downstream experiments were performed 24 h after transfection.

Real-time qPCR analyses

Total RNA was extracted using TRIzol (Takara, Tokyo, Japan), and RNA integrity and concentration were determined by NanoDrop to ensure equal input for each sample. Reverse transcription was performed with All-in-One cDNA Synthesis Supermix (Takara), followed by RT-qPCR using SYBR Green PCR Master Mix (Takara) and specific mouse primers on a LightCycler 480 system. Data were analyzed by the 2 − ΔΔCT method and normalized to GAPDH. Primers are listed below: Myod1-F: TCTATGATGACCCGTGTTTCG; Myod1-R:TGCACCGCAGTAGGGAAGT;Myog-F: CCCTACAGACGCCCACAATC; Myog-R: AAGGCAACAGACATATCCTCCAC; MYH3-F: ATGAGACCGTGGTGGGACTG; MYH3-R: TTGTAGCGAAGGTGGCATAGAG; Lgals3-F: ACCACTGACGGTGCCCTATG; Lgals3-R: GTTTCACTGTGCCCATGATTGT; GAPDH-F: CATCAAGAAGGTGGTGAAGC; GAPDH-R:AAGGTGGAAGAGTGGGAGTT.

Data analysis

All data were analyzed using SPSS (version 24.0; IBM Corp.) and visualized with GraphPad Prism (version 10.1.2; GraphPad Software). Data are presented as mean ± SD. Normality and homogeneity of variance were assessed using the Shapiro-Wilk and Levene's tests, respectively. For two-group comparisons, independent samples t-tests were used when both assumptions were met, Welch's t-test when variances were unequal, and the Mann-Whitney U test when normality was violated. For three or more groups, one-way ANOVA with Tukey's post hoc test was used when assumptions were met, Welch's ANOVA with Games-Howell post hoc test when variances were unequal, and the Kruskal-Wallis test with Dunn's post hoc test (Bonferroni correction) when normality was violated. $P < 0.05$ was considered statistically significant.

Results

1.Dynamic changes of Lgals3 in muscle satellite cells in vitro

Transcriptome profiles of satellite cells at rest and at 3 days post-injury were obtained from a public database and compared. Although fluorescence-activated cell sorting (FACS) may induce partial activation[29], freshly isolated muscle satellite cells (MuSCs) in the dataset were designated as quiescent satellite cells (QSCs), whereas the mixed population of proliferating satellite cells and progenitor cells isolated 3 days after cardiotoxin (CTX) injury was designated as activated satellite cells (ASCs)[30]. QSCs exhibited elevated expression of canonical MuSC markers, including Pax7, CD34[31], and Calcr[32], while proliferation- and mitosis-associated markers such as Mki67 and Cdk1 were expressed at lower levels. Conversely, ASCs showed upregulated expression of genes involved in myogenic differentiation and development, including the myogenic regulator Myod1, myofibrillar assembly markers (e.g., MyHC), and troponin and actin genes. Expression of nine galectin family members (Lgals1–4, 6–9, 12) was detected, among which Lgals3, Lgals4, and Lgals9 exhibited significant differential expression (log2 fold change > 1). Notably, only Lgals3 (Galectin-3) was rapidly and specifically induced in ASCs (Fig. 1A).

To verify the dynamic changes of Lgals3 during muscle satellite cell activation, adult C57 mouse muscle fibers were isolated and cultured in vitro, with muscle satellite cells maintained in their physiological

position. At the time of fresh isolation (0 h), no Lgals3 expression was detected in Pax7 + quiescent MuSCs; however, after 24 h of culture, Lgals3 protein was detected in more than 60% of MuSCs (Fig. 1B, C). To further verify the dynamic changes of Lgals3 during muscle satellite cell activation and differentiation, freshly isolated (FISC), activated (ASC-24 h), proliferated (ASC-48 h), and differentiated (DSC-72 h) satellite cells were obtained by FACS sorting and cultured in vitro for 0, 24, 48, or 72 h[33]. qPCR results showed that Myod1, an early differentiation-related myogenic factor, was barely expressed in FISC but gradually increased in activated (ASC-24 h) and proliferated (ASC-48 h) cells, peaking at ASC-48 h. In contrast, Myog and MYH3, which are associated with late differentiation, increased sharply at DSC-72 h (Fig. 1D–G). The expression pattern of Lgals3 closely resembled that of Myod1 (Fig. 1E). Additionally, changes in Lgals3 during primary myoblast differentiation were examined by qPCR. Myod1 and Myog gradually increased with differentiation, whereas Lgals3 remained unchanged. These results indicate that Lgals3 is absent in resting muscle satellite cells, rapidly induced during activation and proliferation, and maintained during differentiation.

2. Deletion of Lgals3 in satellite cells leads to impaired skeletal muscle regeneration in adult mice

The upregulation of Lgals3 observed during satellite cell activation and proliferation suggests that this event may be important for skeletal muscle development and/or regeneration. To verify this, mice carrying the Pax7 Cre/ERT2 allele were crossed with Lgals3fl/fl mice to generate a muscle satellite cell-specific Lgals3 knockout mouse model (Lgals3scko). 8-week-old Lgals3fl/fl and Lgals3scko mice were intraperitoneally injected with tamoxifen for five consecutive days and fed a tamoxifen-containing diet to induce recombinase activity. Without injury, no significant differences in histological morphology, muscle weight, or muscle fiber cross-sectional area (CSA) were observed between Lgals3scko and control mice (Fig. 2A–C). In addition, the number of resting MuSCs in Lgals3scko mice was comparable to that in control mice (Fig. 2D, E), indicating that Lgals3 is dispensable for muscle development and the maintenance of MuSC quiescence.

Next, the role of Lgals3 in skeletal muscle regeneration was examined. Acute injury was induced by injecting CTX (10 μM, 100 μL) into the tibialis anterior (TA) muscle of adult Lgals3fl/fl and Lgals3scko mice, and muscles were isolated at 3, 5, and 7 days post-injury for H&E staining analysis. The results showed that muscle regeneration was significantly impaired in Lgals3scko mice compared with Lgals3fl/fl mice (Fig. 2F). On day 5 post-injury, numerous newly formed centronuclear fibers (CNFs) appeared in the TA muscle of Lgals3fl/fl mice, whereas signs of TA muscle regeneration in Lgals3scko mice were markedly insufficient, with significant reductions in both CSA and CNF number (Fig. 2G, H). On day 7 post-injury, the CSA of Lgals3scko mice remained significantly lower than that of control mice (Fig. 2G). Although the number of CNFs per field was higher, the proportion of CNFs containing more than one nucleus was not increased (Fig. 2I). These results suggest that loss of Lgals3 in muscle satellite cells significantly impairs skeletal muscle regeneration.

3.Lgals3 deletion inhibits the activation and proliferation of MuSCs during muscle regeneration

In injured muscle of Lgals3scko mice, both the number and size of CNFs were significantly reduced, suggesting that either fewer activated satellite cells participate in myogenesis or that satellite cells harbor intrinsic defects in forming fusion-competent myoblasts. To further investigate this phenomenon, muscle sections from Lgals3scko and Lgals3fl/fl mice were immunostained for Pax7, laminin, and DAPI at 5 days post-injury. The results showed that the number of Pax7 + cells was significantly increased in Lgals3fl/fl muscle, indicating effective satellite cell activation and proliferation, whereas this increase was not significant in Lgals3scko muscle (Fig. 3A, B). In addition, equal numbers of MuSC-derived primary myoblasts from Lgals3fl/fl and Lgals3scko mice were isolated and cultured for 48 h, followed by pulse labeling with 5-ethynyl-2'-deoxyuridine (EdU). The proportion of Pax7 + EdU+ cells was significantly lower in Lgals3scko myoblasts than in Lgals3fl/fl myoblasts (Fig. 3C, D). These results indicate that Lgals3 deletion significantly inhibits MuSC-derived primary myoblast proliferation.

Because MuSCs must exit quiescence and re-enter the cell cycle (i.e., activation) before proliferating, we further investigated whether Lgals3 deletion affects MuSC activation. Myod1 is absent in QSCs but expressed in activated/proliferating MuSCs[34]. After 24 h of culture of freshly isolated muscle fibers, the number of Pax7 + Myod1+ cells was significantly reduced in Lgals3scko mice (Fig. 3E, F). These results indicate that Lgals3 deletion not only inhibits MuSC proliferation but also significantly impairs the activation process, thereby favoring the maintenance of MuSCs in a quiescent state.

4. Lgals3 deletion promotes the proliferation MuSCs to exit the cycle and self-renewal, but inhibits myogenic differentiation

The final step of myogenesis is cell cycle exit and fusion into multinucleated myofibers, while a subset of satellite cells returns to quiescence to replenish the stem cell pool. After freshly isolated MuSC-derived primary myoblasts were cultured for 72 h, over 70% of Lgals3fl/fl cells were Myod1+, versus fewer than 40% of Lgals3scko cells (Fig. 4A, B); similarly, over 80% of Lgals3fl/fl cells were Myog+, versus fewer than 60% of Lgals3scko cells (Fig. 4C, D). Moreover, after 3 days of horse serum-induced differentiation, myotubes formed by Lgals3scko myoblasts were significantly thinner than those of Lgals3fl/fl cells (Fig. 4E, F). Thus, Lgals3 deletion inhibits MuSC myogenic differentiation.

Lgals3 deletion increased the proportion of Pax7 + EdU− cells, suggesting a role for Lgals3 in skeletal muscle regeneration and MuSC re-entry into quiescence (self-renewal) in vitro. To this end, single muscle fibers were cultured under normoxia for 72 h. MuSC activation and proliferation generated MuSC clusters on the fibers, which were stained for Pax7 and Myod1 (Fig. 4G). Compared with control fibers, DAPI+ nuclei per MuSC cluster were significantly reduced after Lgals3 knockout, supporting the notion that Lgals3 knockout promotes MuSC quiescence and hinders proliferation (Fig. 4H). In addition, Pax7 + Myod1− self-renewing MuSCs increased in Lgals3scko muscle fibers, whereas Pax7 − Myod1+ myoblasts decreased. Thus, Lgals3 knockout inhibits myogenic differentiation but promotes self-renewal (Fig. 4I–K).

To confirm that these effects are MuSC-independent, primary myoblasts from Lgals3fl/fl and Lgals3scko mice were differentiated in 2% horse serum for 5 days and stained for Pax7 and myosin heavy chain

(MyHC). Lgals3scko myoblasts were either Pax7 + MyHC− (self-renewal reserve cells) or Pax7 − MyHC+ (differentiated cells), whereas almost all WT cells were MyHC+, confirming that Lgals3 deletion hinders myoblast differentiation but promotes self-renewal (Fig. 4L–N).

5.Lgals3 deletion induces mitochondrial fragmentation through interaction with Drp1

To further explore the biological function of Lgals3 in myoblasts, we identified its interaction partners by pull-down coupled with mass spectrometry (MS). Cell component enrichment analysis showed that a series of mitochondrial proteins co-purified with Lgals3 (~ 10% of the total; Fig. 5A, Supplementary Table). Molecular function enrichment revealed that Lgals3-interacting proteins were enriched in guanosine acid binding, GTPase binding, and NADH redox activity (Fig. 5B), while biological process enrichment implicated them in energy metabolism pathways (Fig. 5C). We first assessed the effect of Lgals3 deletion on overall mitochondrial morphology in myoblasts. Freshly isolated myoblasts were cultured for 2 days. Under control conditions, Mitotracker-stained mitochondria appeared as a sparse network around the nucleus, consistent with previous studies[35, 36]. In Lgals3-deleted cells, mitochondria were fragmented (Fig. 5D), and mitochondrial footprint, average branch length, and median branch length were significantly reduced in Lgals3scko cells (Fig. 5E–G). These results suggest that Lgals3 deficiency causes mitochondrial fragmentation.

We then searched the pull-down MS data for potential targets that interact with Lgals3 and regulate mitochondrial fission. GTPase-driven signaling is key to regulating mitochondrial fission and fusion and serves as an upstream mediator of cell metabolism[37]. Our MS results showed that Lgals3 interacts with multiple GTPases, among which Dnm1l (Drp1), a major driver of mitochondrial fission that also plays an important role in myogenesis[38, 39], was particularly notable. Molecular docking simulation indicated that Lgals3 could bind Drp1 (Fig. 5H), and co-IP further verified this interaction (Fig. 5I). To clarify the role of Drp1 in Lgals3 knockout-induced mitochondrial fission, Drp1 siRNA was transfected into Lgals3scko cells. Immunofluorescence showed that, consistent with previous results, mitochondrial fission was increased in Lgals3scko cells, whereas simultaneous depletion of Lgals3 and Drp1 reduced fission (Fig. 5J) and significantly increased mitochondrial footprint (Fig. 5K). These results suggest that Lgals3 knockout-induced mitochondrial fission is mediated by Drp1.

6.Lgals3 deletion induced mitochondrial fragmentation reduced energy production and inhibited autophagy

Given that mitochondria are a major energy source for cells, we examined the effect of Lgals3 deletion-induced mitochondrial fragmentation on ATP production and observed a significant decrease in ATP levels in Lgals3scko cells (Fig. 6A). Mitochondrial fission, a prerequisite for proper organelle segregation between daughter cells during mitosis, is important for muscle satellite cell expansion and skeletal muscle regeneration[40], but can also trigger apoptosis or mitophagy[41, 42]. Our results showed that MuSC proliferation decreased after Lgals3 knockout, we therefore examined whether Lgals3 knockout alters apoptosis and autophagy in myoblasts. The results showed that cleaved caspase-3 did not

decrease in Lgals3scko cells, whereas LC3-II and p62, two major autophagy markers, exhibited autophagic accumulation (Fig. 6B–E).

Discussion

We confirmed the key role of Lgals3 in regulating muscle satellite cell function. In vivo, MuSC-specific Lgals3 knockout impaired skeletal muscle regeneration, whereas in vitro, MuSCs lacking Lgals3 exhibited significantly reduced activation, proliferation, and myogenic differentiation. These findings are highly consistent with those of Cerri et al.[43], who used an Lgals3 knockout mouse model to demonstrate that expression of myogenic factors such as Myod1 and Myog was significantly downregulated after skeletal muscle injury, indicating that Lgals3 is indispensable for regulating myogenic gene expression. Notably, although Lgals3 loss impairs MuSC activation, proliferation, and differentiation, self-renewal is significantly enhanced, suggesting that Lgals3 may influence the balance between MuSC self-renewal and differentiation by regulating cell fate-determining factors. Cerri et al. provided further evidence, showing that Lgals3 knockout myoblasts maintained high Pax7 expression during proliferation, consistent with our observation of enhanced self-renewal. Collectively, these data indicate that Lgals3 is not merely a passive marker of MuSC activation but an active regulator that coordinates the divergent fate choices of MuSCs during regeneration.

Mechanistically, our study reveal a previously unrecognized link between Lgals3, mitochondrial dynamics, and MuSC fate determination. Mitochondrial dynamics play a crucial role in the regulation of muscle generation and the fate of muscle satellite cells. For example, OPA1 inhibition reduces muscle stem cell number and causes abnormal mitochondrial morphology[44], whereas Drp1 inhibition in C2C12 cells reduces mitochondrial fission and impairs myogenic differentiation[36]. Our research shows that upon Lgals3 knockout, mitochondrial fission increased and mitochondrial branch length decreased significantly relative to control cells, consistent with epithelial cell data reported by Coppin et al.[45]. Specifically, Lgals3 interacts with Drp1, and knockout of both maintains mitochondrial reticular structure. Thus, Lgals3 regulates mitochondrial dynamics through Drp1. Notably, mitochondrial fission is required for mitosis; reduced fission caused by Drp1 knockout leads to inefficient oxidative phosphorylation (OXPHOS) and mitophagy, decreasing satellite cell proliferation and impairing muscle regeneration[46]. However, in our study, although mitochondrial fission increased after Lgals3 knockout, cell proliferation decreased. We speculate that the increased mitochondrial fission is not mitotic midzone division but peripheral division[47]. Both modes require Drp1; the former supports normal mitochondrial division during active metabolism (e.g., cell proliferation), whereas the latter represents a protective response that clears damaged mitochondria and prevents cell death by triggering autophagy under stress. This type of peripheral division may reflect enhanced autophagic flux in MuSCs, thereby favoring the maintenance of quiescence rather than promoting activation or proliferation. Further analysis confirmed that Lgals3 knockout promotes autophagy.

Based on these findings, Lgals3 may act as a "molecular switch" in MuSCs, whereby targeted regulation of its expression could precisely control MuSC fate. This discovery not only deepens our understanding of MuSC biology but also provides new insights for developing MuSC-based regenerative medicine strategies.

Conclusion

Lgals3 is rapidly induced upon MuSC activation and is essential for skeletal muscle regeneration by promoting MuSC activation, proliferation, and myogenic differentiation while limiting self-renewal. Mechanistically, Lgals3 interacts with Drp1 to regulate mitochondrial fission and autophagy, thereby acting as a molecular switch in MuSC fate determination.

Declarations

Ethics Statement

All animal studies have been approved by the appropriate ethics committee and have therefore been performed in accordance with the ethical standards laid down in the 1964 Declaration of Helsinki and its later amendments.

Conflicts of Interest

The authors declare no conflicts of interest.

Acknowledgements

This work is supported by the Chongqing Postdoctoral Science Foundation (CSTB2023NSCQ-BHX0057) and the Chongqing Municipal Education Commission Foundation (Youth Program, KJQN202502827).

Availability of Data and Materials:

The data that support the findings of this study are available from the corresponding author upon reasonable request.

References

1. Sayer A A, Cooper R, Arai H, et al. Sarcopenia[J]. Nat Rev Dis Primers, 2024,10(1):68.
2. Qiao R, Guo J, Zhang C, et al. Diabetes-induced muscle wasting: molecular mechanisms and promising therapeutic targets[J]. Crit Rev Food Sci Nutr, 2025,65(20):4007–4023.

3. Huot J R, Baumfalk D, Resendiz A, et al. Targeting Mitochondria and Oxidative Stress in Cancer- and Chemotherapy-Induced Muscle Wasting[J]. Antioxid Redox Signal, 2023,38(4–6):352–370.
4. Gowda C, Brown T T, Compher C, et al. Prevalence and predictors of low muscle mass in HIV/viral hepatitis coinfection[J]. AIDS, 2016,30(16):2519–2528.
5. Dumont N A, Bentzinger C F, Sincennes M, et al. Satellite Cells and Skeletal Muscle Regeneration[J]. Compr Physiol, 2015,5(3):1027–1059.
6. Tedesco F S, Dellavalle A, Diaz-Manera J, et al. Repairing skeletal muscle: regenerative potential of skeletal muscle stem cells[J]. J Clin Invest, 2010,120(1):11–19.
7. Giordani L, Parisi A, Le Grand F. Satellite Cell Self-Renewal[J]. Curr Top Dev Biol, 2018,126:177–203.
8. Morgan J E, Zammit P S. Direct effects of the pathogenic mutation on satellite cell function in muscular dystrophy[J]. Exp Cell Res, 2010,316(18):3100–3108.
9. Sacco A, Mourkioti F, Tran R, et al. Short telomeres and stem cell exhaustion model Duchenne muscular dystrophy in mdx/mTR mice[J]. Cell, 2010,143(7):1059–1071.
10. Garcia-Prat L, Martinez-Vicente M, Perdiguero E, et al. Autophagy maintains stemness by preventing senescence[J]. Nature, 2016,529(7584):37–42.
11. Sousa-Victor P, Gutarra S, Garcia-Prat L, et al. Geriatric muscle stem cells switch reversible quiescence into senescence[J]. Nature, 2014,506(7488):316–321.
12. Sousa-Victor P, Garcia-Prat L, Munoz-Canoves P. Control of satellite cell function in muscle regeneration and its disruption in ageing[J]. Nat Rev Mol Cell Biol, 2022,23(3):204–226.
13. Montarras D, Morgan J, Collins C, et al. Direct isolation of satellite cells for skeletal muscle regeneration[J]. Science, 2005,309(5743):2064–2067.
14. Vilquin J T. Myoblast transplantation: clinical trials and perspectives. Mini-review[J]. Acta Myol, 2005,24(2):119–127.
15. Mendell J R, Kissel J T, Amato A A, et al. Myoblast transfer in the treatment of Duchenne's muscular dystrophy[J]. N Engl J Med, 1995,333(13):832–838.
16. Liu F, Stowell S R. The role of galectins in immunity and infection[J]. Nat Rev Immunol, 2023,23(8):479–494.
17. Goldring K, Jones G E, Thiagarajah R, et al. The effect of galectin-1 on the differentiation of fibroblasts and myoblasts in vitro[J]. J Cell Sci, 2002,115(Pt 2):355–366.
18. Ahmed H, Du S, Vasta G R. Knockdown of a galectin-1-like protein in zebrafish (Danio rerio) causes defects in skeletal muscle development[J]. Glycoconj J, 2009,26(3):277–283.
19. Ding Z, Liu X, Ren X, et al. Galectin-1-induced skeletal muscle cell differentiation of mesenchymal stem cells seeded on an acellular dermal matrix improves injured anal sphincter[J]. Discov Med, 2016,21(117):331–340.
20. Blazev R, Ashwood C, Abrahams J L, et al. Integrated Glycoproteomics Identifies a Role of N-Glycosylation and Galectin-1 on Myogenesis and Muscle Development[J]. Molecular & cellular proteomics: MCP, 2021,20:100030.

21. Rancourt A, Dufresne S S, St-Pierre G, et al. Galectin-3 and N-acetylglucosamine promote myogenesis and improve skeletal muscle function in the mdx model of Duchenne muscular dystrophy[J]. FASEB J, 2018,32(12):fj201701151R.
22. Cerri D G, Rodrigues L C, Alves V M, et al. Endogenous galectin-3 is required for skeletal muscle repair[J]. Glycobiology, 2021,31(10):1295–1307.
23. Soares L C, Al-Dalahmah O, Hillis J, et al. Novel Galectin-3 Roles in Neurogenesis, Inflammation and Neurological Diseases[J]. Cells, 2021,10(11):3047.
24. Al-Salam S, Jagadeesh G S, Sudhadevi M, et al. Galectin-3 and Autophagy in Renal Acute Tubular Necrosis[J]. International journal of molecular sciences, 2024,25(7):3604.
25. Yang R Y, Liu F T. Galectins in cell growth and apoptosis[J]. Cellular and molecular life sciences: CMLS, 2003,60(2):267–276.
26. Fu X, Li S, Jia M, et al. Induction of Skeletal Muscle Injury by Intramuscular Injection of Cardiotoxin in Mouse[J]. Bio Protoc, 2023,13(9):e4668.
27. Gallot Y S, Hindi S M, Mann A K, et al. Isolation, Culture, and Staining of Single Myofibers[J]. Bio Protoc, 2016,6(19).
28. Valente A J, Maddalena L A, Robb E L, et al. A simple ImageJ macro tool for analyzing mitochondrial network morphology in mammalian cell culture[J]. Acta histochemica, 2017,119(3):315–326.
29. Machado L, Esteves De Lima J, Fabre O, et al. In Situ Fixation Redefines Quiescence and Early Activation of Skeletal Muscle Stem Cells[J]. Cell reports, 2017,21(7):1982–1993.
30. Oprescu S N, Yue F, Qiu J, et al. Temporal Dynamics and Heterogeneity of Cell Populations during Skeletal Muscle Regeneration[J]. iScience, 2020,23(4):100993.
31. García-Prat L, Perdiguero E, Alonso-Martín S, et al. FoxO maintains a genuine muscle stem-cell quiescent state until geriatric age[J]. Nature cell biology, 2020,22(11):1307–1318.
32. Baghdadi M B, Castel D, Machado L, et al. Reciprocal signalling by Notch-Collagen V-CALCR retains muscle stem cells in their niche[J]. Nature, 2018,557(7707):714–718.
33. Zhang S, Yang F, Huang Y, et al. ATF3 induction prevents precocious activation of skeletal muscle stem cell by regulating H2B expression[J]. Nat Commun, 2023,14(1):4978.
34. Zammit P S, Golding J P, Nagata Y, et al. Muscle satellite cells adopt divergent fates: a mechanism for self-renewal?[J]. The Journal of cell biology, 2004,166(3):347–357.
35. Gasier H G, Dohl J, Suliman H B, et al. Skeletal muscle mitochondrial fragmentation and impaired bioenergetics from nutrient overload are prevented by carbon monoxide[J]. American journal of physiology. Cell physiology, 2020,319(4):C746-C756.
36. Rahman F A, Friedrich Yap J M, Joseph T M, et al. DNM1L-mediated fission governs mitophagy & mitochondrial biogenesis during myogenic differentiation[J]. Cell communication and signaling: CCS, 2025,23(1):158.
37. van der Bliek A M, Shen Q, Kawajiri S. Mechanisms of mitochondrial fission and fusion[J]. Cold Spring Harbor perspectives in biology, 2013,5(6):a011072.

38. Kim B, Kim J, Yoon Y, et al. Inhibition of Drp1-dependent mitochondrial division impairs myogenic differentiation[J]. American journal of physiology. Regulatory, integrative and comparative physiology, 2013,305(8):R927-R938.
39. Bloemberg D, Quadrilatero J. Effect of mitochondrial fission inhibition on C2C12 differentiation[J]. Data in brief, 2016,7:634–640.
40. Yamano K, Youle R J. Coupling mitochondrial and cell division[J]. Nature cell biology, 2011,13(9):1026–1027.
41. Jahani-Asl A, Slack R S. The phosphorylation state of Drp1 determines cell fate[J]. EMBO reports, 2007,8(10):912–913.
42. Mao K, Klionsky D J. Participation of mitochondrial fission during mitophagy[J]. Cell cycle (Georgetown, Tex.), 2013,12(19):3131–3132.
43. Cerri D G, Rodrigues L C, Alves V M, et al. Endogenous galectin-3 is required for skeletal muscle repair[J]. Glycobiology, 2021,31(10):1295–1307.
44. Tezze C, Romanello V, Desbats M A, et al. Age-Associated Loss of OPA1 in Muscle Impacts Muscle Mass, Metabolic Homeostasis, Systemic Inflammation, and Epithelial Senescence[J]. Cell metabolism, 2017,25(6):1374–1389.
45. Coppin L, Jannin A, Ait Yahya E, et al. Galectin-3 modulates epithelial cell adaptation to stress at the ER-mitochondria interface[J]. Cell death & disease, 2020,11(5):360.
46. Hong X, Isern J, Campanario S, et al. Mitochondrial dynamics maintain muscle stem cell regenerative competence throughout adult life by regulating metabolism and mitophagy[J]. Cell stem cell, 2022,29(9):1298–1314.
47. Kleele T, Rey T, Winter J, et al. Distinct fission signatures predict mitochondrial degradation or biogenesis[J]. Nature, 2021,593(7859):435–439.

Figures

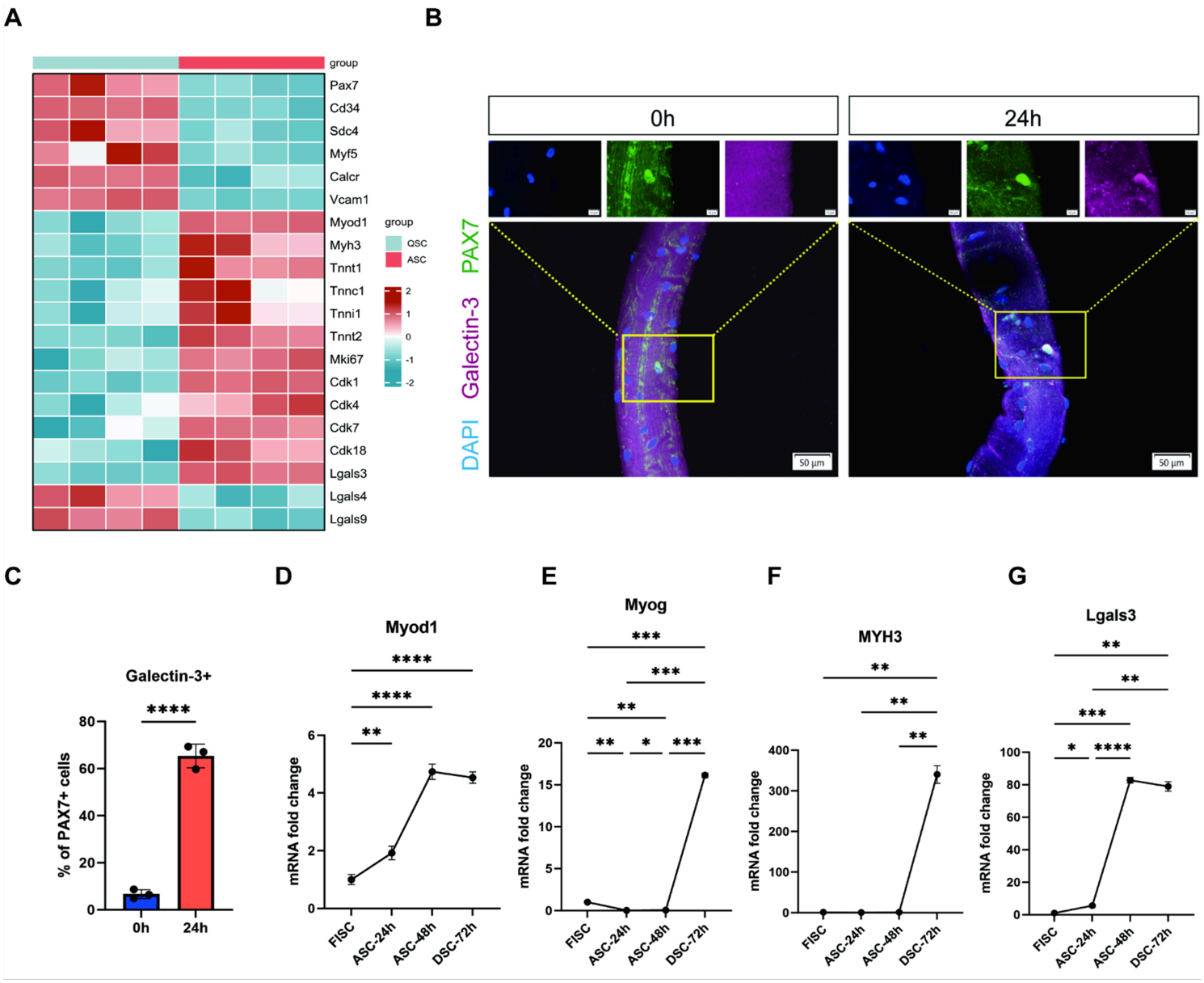


Figure 1

Dynamic expression of Lgals3 during MuSC activation and differentiation.

(A) Heatmap of differentially expressed galectin family members in quiescent satellite cells (QSCs) and activated satellite cells (ASCs) isolated 3 days post-injury, based on transcriptome analysis. Lgals3 was rapidly and specifically induced in ASCs (log2 fold change > 1).

(B, C) Immunofluorescence of single muscle fibers cultured for 0 h and 24 h. **(B)**Representative images showing Pax7 (red), Lgals3 (green), and DAPI (blue). Scale bar = 50 µm. **(C)** Quantification of the percentage of Pax7+ MuSCs expressing Lgals3 at 0 h and 24 h. Data are presented as mean ± SD. n = 3 mice per group, with at least 20 myofibers analyzed per mouse. ****P < 0.0001.

(D–G) qPCR analysis of freshly isolated (FISC), activated (ASC-24 h), proliferated (ASC-48 h), and differentiated (DSC-72 h) satellite cells. Relative mRNA levels of **(D)**Myod1, **(E)** Myog, **(F)** MYH3, and **(G)**

Lgals3, normalized to GAPDH. Data are presented as mean ± SD. n = 3 independent experiments. *P < 0.05, **P < 0.01, ***P < 0.001, ****P < 0.0001.

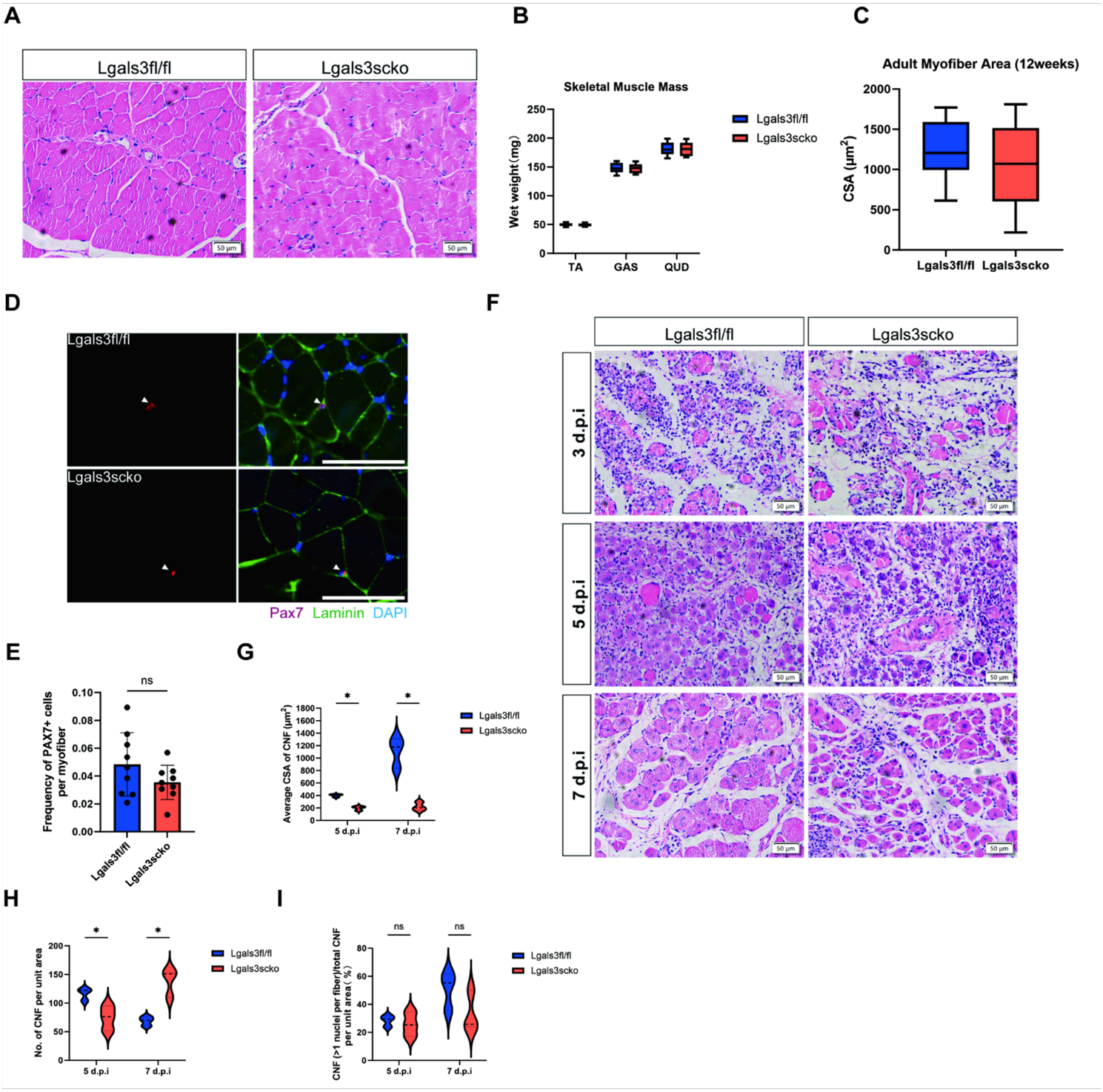


Figure 2

MuSC-specific Lgals3 knockout impairs skeletal muscle regeneration.

(A) Representative H&E-stained cross-sections of uninjured tibialis anterior (TA) muscles from Lgals3fl/fl and Lgals3scko mice. Scale bar = 50 µm.

(B) Muscle weight of TA, gastrocnemius (Gas), and quadriceps (QUD) muscles from uninjured Lgals3fl/fl and Lgals3scko mice. Data are presented as mean ± SD. n = 10 mice per group.

(C) Quantification of muscle fiber cross-sectional area (CSA) in uninjured TA muscles. Data are presented as mean ± SD. n = 3 mice per group.

(D, E) Quantification of resting MuSCs in uninjured TA muscles. **(D)**Representative immunofluorescence images of Pax7 (red), laminin (green), and DAPI (blue). Arrowheads indicate Pax7+ cells. Scale bar = 50 μm. **(E)**Quantification of Pax7+ cells per fiber. Data are presented as mean ± SD. n = 3 mice per group. n.s., not significant.

(F–I) Analysis of TA muscle regeneration at 3, 5, and 7 days post-CTX injury. **(F)**Representative H&E-stained cross-sections at 3, 5, and 7 days post-injury. Scale bar = 50 μm. **(G)** Quantification of CSA at days 5 and 7 post-injury. **(H)** Quantification of CNF number per field at days 5 and 7 post-injury. **(I)** Quantification of CNFs containing more than one nucleus at day 7 post-injury. Data are presented as mean ± SD. n = 3 mice per group. n.s., not significant; *P < 0.05.

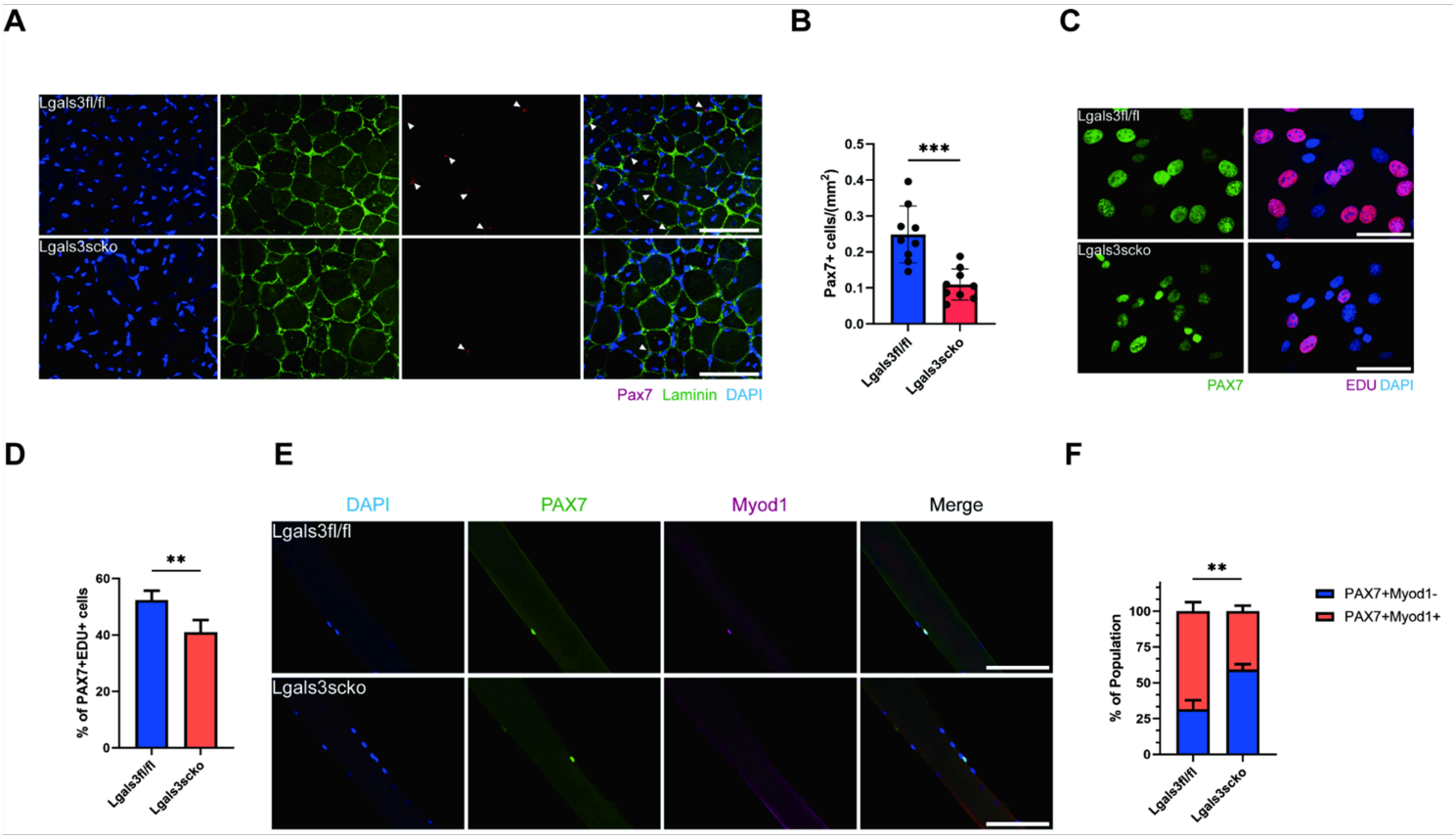


Figure 3

Lgals3 deletion inhibits MuSC activation and proliferation during muscle regeneration.

(A, B) Immunofluorescence of TA muscle sections at 5 days post-injury. **(A)** Representative images showing Pax7 (red), laminin (green), and DAPI (blue). Arrowheads indicate Pax7+ cells. Scale bar = 50

μm. **(B)** Quantification of Pax7+ cells. Data are presented as mean ± SD. n = 3 mice per group. ***P < 0.001.

(C, D) EdU incorporation assay in MuSC-derived primary myoblasts cultured for 48 h. **(C)**Representative images showing Pax7 (green), EdU (red), and DAPI (blue). Scale bar = 50 μm. **(D)** Quantification of Pax7+EdU+ cells. Data are presented as mean ± SD. n = 3 independent experiments. **P < 0.01.

(E, F) Immunofluorescence of single muscle fibers cultured for 24 h. **(E)** Representative images showing Pax7 (green), Myod1 (red), and DAPI (blue). Scale bar = 50 μm. **(F)** Quantification of Pax7+Myod1+ cells. Data are presented as mean ± SD. n = 3 mice per group, with at least 20 myofibers analyzed per mouse. **P < 0.01.

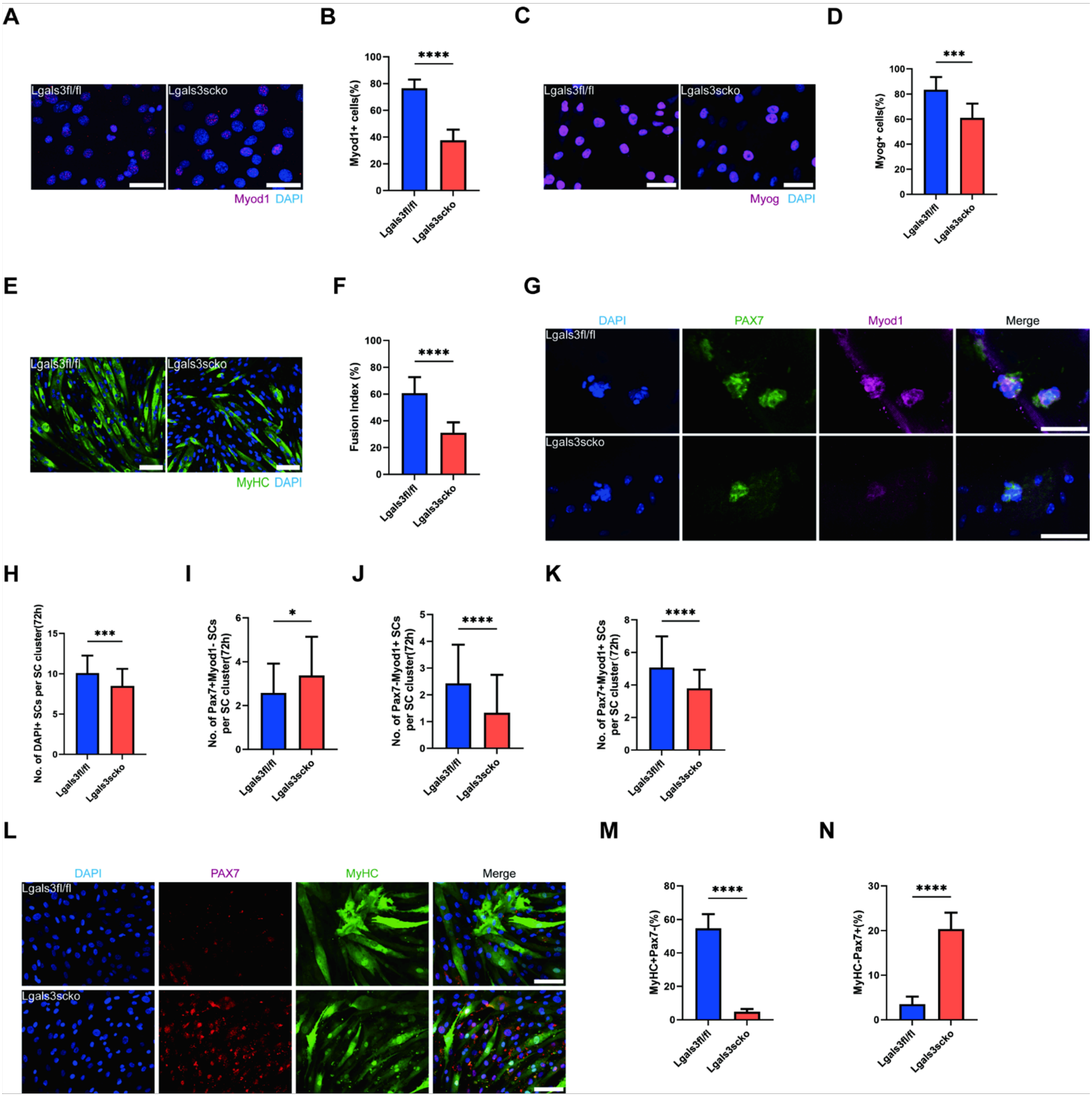


Figure 4

Lgals3 deletion promotes MuSC cell cycle exit and self-renewal but inhibits myogenic differentiation.

(A–D) Immunofluorescence of MuSC-derived primary myoblasts cultured for 72 h. **(A)** Representative images of Myod1 (red) and DAPI (blue); scale bar = 50 μm. **(B)**Quantification of Myod1+ cells. **(C)** Representative images of Myog (red) and DAPI (blue); scale bar = 50 μm. (D) Quantification of Myog+ cells. Data are mean ± SD; n = 3 independent experiments. ***P < 0.001, ****P < 0.0001.

(E, F) Differentiation of MuSC-derived primary myoblasts in 2% horse serum for 3 days. **(E)** Representative images of myotubes stained for MyHC (green) and DAPI (blue); scale bar = 50 μm. **(F)** Quantification of fusion index. Data are mean ± SD; n = 3 independent experiments. ****P < 0.0001.

(G–K) MuSC self-renewal on single muscle fibers cultured for 72 h. **(G)**Representative images of Pax7 (green), Myod1 (red), and DAPI (blue); scale bar = 50 μm. **(H)** DAPI+ nuclei per MuSC cluster. **(I)** Pax7+Myod1− self-renewing MuSCs per cluster. **(J)** Pax7−Myod1+ myoblasts per cluster. **(K)**Pax7+Myod1+ MuSCs per cluster. Data are mean ± SD; n = 3 mice per group. *P < 0.05, ***P < 0.001, ****P < 0.0001.

(L–N) Self-renewal of primary myoblasts in 2% horse serum for 5 days. **(L)** Representative images of Pax7 (red), MyHC (green), and DAPI (blue); scale bar = 50 μm. **(M)**Pax7+MyHC− reserve cells. **(N)** Pax7−MyHC+ differentiated cells. Data are mean ± SD; n = 3 independent experiments. ****P < 0.0001.

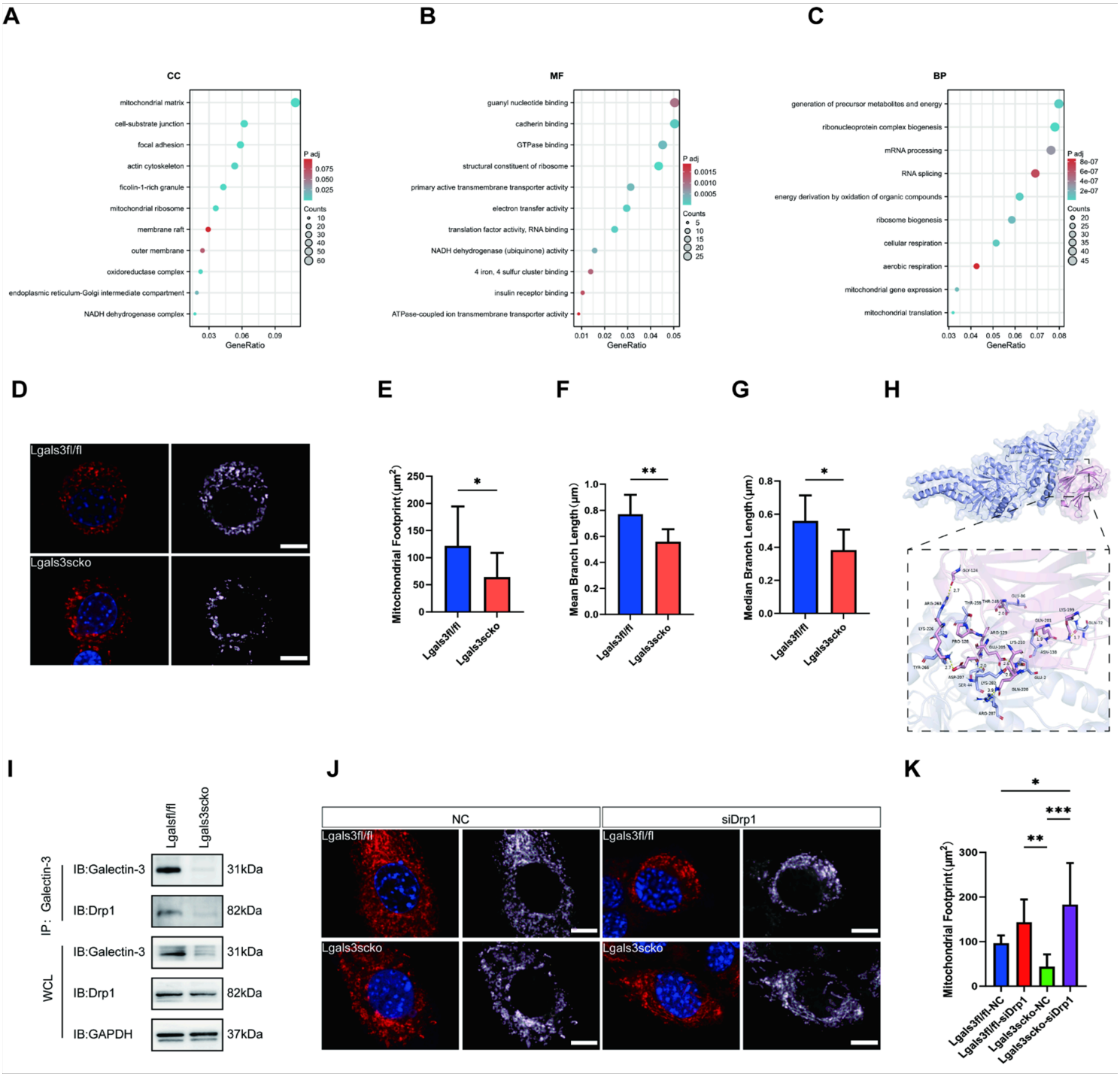


Figure 5

Lgals3 interacts with Drp1 and regulates mitochondrial fission.

(A–C) Pull-down coupled with mass spectrometry (MS) analysis of Lgals3-interacting proteins in myoblasts. **(A)** Cellular Component (CC) enrichment. **(B)** Molecular Function (MF) enrichment. **(C)** Biological Process (BP) enrichment. n = 3 mice per group.

(D–G) Mitochondrial morphology analysis in Lgals3fl/fl and Lgals3scko myoblasts cultured for 2 days. **(D)** Representative images of Mito-Tracker Red-stained mitochondria, scale bar=10μm. **(E)** Mitochondrial

footprint. **(F)** Average branch length. **(G)** Median branch length. Data are presented as mean ± SD. n = 3 independent experiments. *P < 0.05, **P < 0.01.

(H, I) Validation of Lgals3–Drp1 interaction. **(H)**Molecular docking simulation of Lgals3 and Drp1. **(I)** Co-IP analysis of Lgals3 and Drp1 in myoblasts.

(J, K) Mitochondrial morphology in Lgals3scko myoblasts transfected with Drp1 siRNA. **(J)**Representative images of Mito-Tracker Red-stained mitochondria, scale bar=10μm. **(K)** Quantification of mitochondrial footprint. Data are presented as mean ± SD. n = 3 independent experiments. *P < 0.05, **P < 0.01,***P < 0.001.

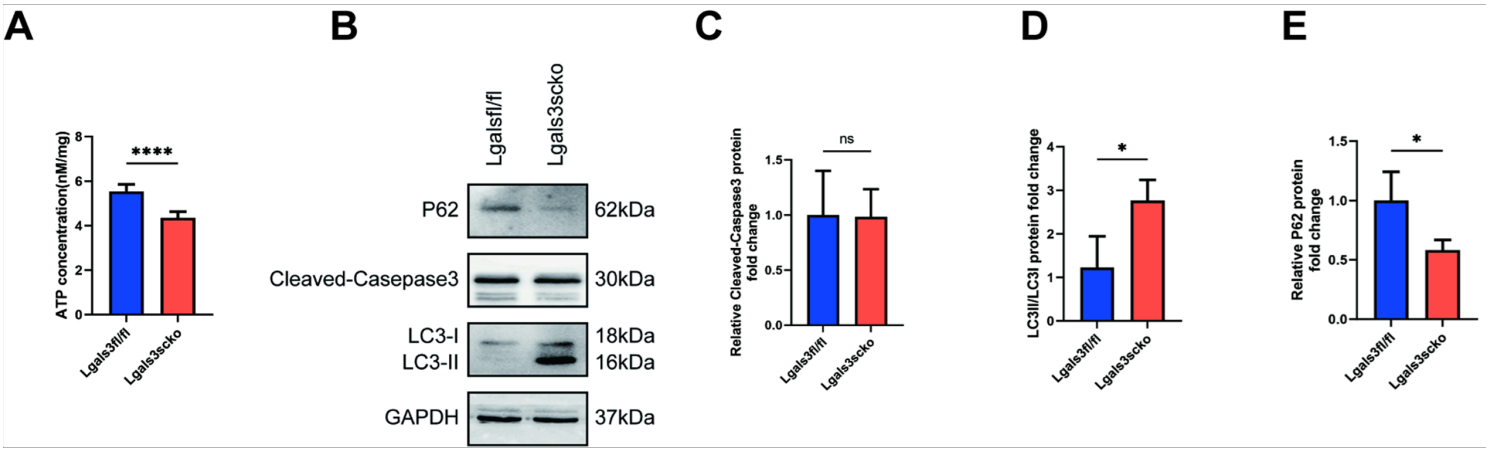


Figure 6

Lgals3 deletion reduces ATP production and promotes autophagy.

(A) ATP levels in Lgals3fl/fl and Lgals3scko myoblasts. Data are presented as mean ± SD. n = 3 independent experiments. ****P < 0.0001.

(B–E) Western blot analysis of apoptosis and autophagy markers in Lgals3fl/fl and Lgals3scko myoblasts. **(B)** Representative immunoblots of cleaved caspase-3, LC3-II/I, p62, and GAPDH. **(C–E)** Quantification of **(C)** cleaved caspase-3, **(D)**LC3-II/I, and **(E)** p62 relative to GAPDH. Data are presented as mean ± SD. n = 3 independent experiments. *P < 0.05; n.s., not significant.

Supplementary Files

This is a list of supplementary files associated with this preprint. Click to download.

- SupplementaryTable.xlsx
- OriginalwesternblotsFig5.tif
- OriginalwesternblotsFig6.tif